Article

Journal of the Brazilian Chemical Society

https://dx.doi.org/10.21577/0103-5053.20230151

J. Braz. Chem. Soc. **2024**, *35*, 4, e-20230151, 1-15

Exploring Urease Inhibition by Coumarin Derivatives through *in silico* and *in vitro* Methods

Marciéli Fabris, [a] ***Priscila G. Camargo,*** [b] ***Mariana L. Silva,*** [a] ***Talis U. Silva,*** [c] ***Sérgio P. Machado,*** [c] ***Carlos R. Rodrigues,*** [b] ***Camilo H. S. Lima,*** [c] ***Magaly G. Albuquerque*** [c] ***and Marcelle L. F. Bispo*** *,[a]

[a]*Laboratório de Síntese de Moléculas Medicinais (LaSMMed), Departamento de Química, Centro de Ciências Exatas, Universidade Estadual de Londrina, Celso Garcia CID, Campus Universitário, 86057-970 Londrina-PR, Brazil*

[b]*Faculdade de Farmácia, Departamento de Fármacos e Medicamentos, Universidade Federal do Rio de Janeiro, Avenida Carlos Chagas Filho, Cidade Universitária, 21941-902 Rio de Janeiro-RJ, Brazil*

[c]*Instituto de Química, Centro de Ciências Matemáticas e da Natureza, Universidade Federal do Rio de Janeiro, Avenida Athos da Silveira Ramos, Cidade Universitária, 21941-909 Rio de Janeiro-RJ, Brazil*

In this report, we designed and synthesized ten *N*-(R-phenyl)-3-carboxamide-coumarin derivatives (**2a-2j**), exploring the coumarin nucleus, and an R-phenyl group as a structural scaffold and a peptide bond as a linker between them. The structure-activity relationships were investigated with different R-substituents (H, Br, NO_2, Cl) in *ortho*, *meta*, or *para* positions from the phenyl group. Coumarins were obtained in good yields (72-95%), and *in vitro* screening against *Canavalia ensiformis* urease showed potential inhibitory percentages ranging from 42 to 65%. Half-maximal inhibitory concentration (IC_{50}) values were determined for the best compounds **2b** (R = 2-Br) and **2d** (R = 4-Br). After conducting molecular docking and molecular dynamics on urease from *C. ensiformis* and *Helicobacter pylori*, potential binding modes for the most effective compounds **2b** and **2d** showed that these derivatives are able to interact with the crucial residue Cys592, thereby blocking the access of the urea substrate to the active site. According to density functional theory (DFT) calculations, 4-Br substitution on *H. pylori* urease was necessary for interacting with catalytic amino acids on the active site.

Keywords: *Canavalia ensiformis*, *Helicobacter pylori*, molecular docking, DFT, molecular dynamics

Introduction

Ureases (EC 3.5.1.5, urea amidohydrolases) are nickel-dependent metalloenzymes that catalyze the hydrolysis of urea, producing ammonium bicarbonate after spontaneous decomposition, generating carbon dioxide, ammonia, and water.[1] This enzyme can be present in large quantities in plants such as *Canavalia ensiformis*, animal tissues, and many microorganisms such as fungi and bacteria.[2-4] Due to its catalytic activity, ureases are related to several health problems, such as stomach cancer, peptic ulceration, pyelonephritis, or cryptococcosis, caused by pathogenic ureolytic microorganisms.[5] For example, the Gram-negative bacterium *Helicobacter pylori* uses urease as a virulence factor since the products from catalytic hydrolyses, mainly ammonia and carbamate, increase the pH of the stomach, and then this neutralizing effect supports its survival and colonization of gastric mucosa.[6] Therefore, urease inhibition is considered a promising strategy for searching for new and effective inhibitors to treat diseases caused by pathogenic microorganisms.

Several urease inhibitors have been reported in the literature due to their potential to inhibit urease *in vitro*,[7-10] including compounds containing coumarin scaffold. Among them are bis-coumarins,[11,12] coumarinyl pyrazolinyl

*e-mail: mlfbispo@uel.br
Editor handled this article: Brenno A. D. Neto

thioamide derivatives,[13] and hybrids featuring coumarin and thiazolotriazole[14] that showed excellent results against urease from *Canavalia ensiformis* (CEU) when compared to the standard thiourea inhibitor. Based on this potential exhibited by coumarin derivatives as urease inhibitors, we decided to synthesize a series of ten *N*-(R-phenyl)-3-carboxamide-coumarin derivatives (**2a-2j**, R = H, Br, NO_2, Cl) and evaluate them *in vitro* against CEU urease.

Our series involves a peptide bond as a linker (shown in blue in Figure 1) to a phenyl group. The phenyl group has substituents at *ortho*-, *meta*-, or *para*-positions with varying steric and electronic properties, such as Cl, Br, or NO_2, aiming to explore the structure-activity relationship (SAR). Furthermore, our goal is to explore the potential pharmacophore role of the coumarin nucleus, which is highlighted in red in Figure 1. This is because these particular coumarins have yet to be recognized in the literature as inhibitors of CEU compounds. Another hypothesis being investigated is the potential connection between the coumarin core that contains a Michael acceptor group (indicated with dashed lines in Figure 1) and its susceptibility to a nucleophilic attack from the free thiol group of Cys592. For this purpose, we applied *in silico* methods, such as density functional theory (DFT), molecular docking, and molecular dynamics studies, to explore putative binding modes on CEU and *Helicobacter pylori* ureases (HPU) (Figure 1).

Experimental

General procedures

Solvents were used without further purification, except for acetone which was dried on a 3 Å molecular sieve for 4-6 h before use. Melting points were recorded on a hot plate apparatus (MQAPF-302, Microquímica Equipamentos Ltda, Palhoça, Brazil) and are uncorrected. The mass spectra were obtained in gas chromatography coupled to a mass spectrometer (GC-MS) Shimadzu (Kyoto, Japan) model GCMS-QP5000, 99604. ^{1}H nuclear magnetic resonance (NMR) spectra were recorded on a Bruker Avance III (Billerica, USA) operating at 400 MHz using a 5 mm broadband probe and $CDCl_3$ as solvent. Chemical shifts (δ in ppm) were referenced to the residual solvent signal ($CHCl_3$ in $CDCl_3$ at δ 7.26). Abbreviations used in the description of the splitting of proton resonances: s (singlet), d (doublet), t (triplet), q (quartet), m (multiplet), Ar (aromatic). Coupling constants (*J*) are reported in Hz.

Synthesis of coumarin-3-carboxylic acid (**1**)

Starting material was synthesized according to the method described by Deshmukh *et al.*[15] Briefly, 2-hydroxybenzaldehyde (7.00 mmol) was dissolved in 25 mL of distilled water, followed by the addition of Meldrum's acid (7.01 mmol). The reaction mixture remained under stirring and heating at 75 °C for 4 h. Then, the reaction mixture was cooled to room temperature, and the white precipitate was filtered under a vacuum and washed with ice-cold distilled water (3 × 5 mL).

White solid; 92% yield; mp 191 °C; lit. 191-192 °C; MS *m/z*, 190 (35%), 146 (100%); ^{1}H NMR (400.1 MHz, $CDCl_3$) δ 12.21 (1H, s, OH), 8.95 (1H, s, H4), 7.82-7.76 (2H, m, H5 and H7), 7.52-7.47 (2H, m, H6 and H8);[15] ^{13}C NMR (100.6 MHz, $CDCl_3$) δ 164.20 (C), 162.5 (C), 154.7 (C), 151.6 (C), 135.9 (C), 130.6 (CH), 126.4 (CH), 118.6 (CH), 117.3 (CH), 115.0 (CH).

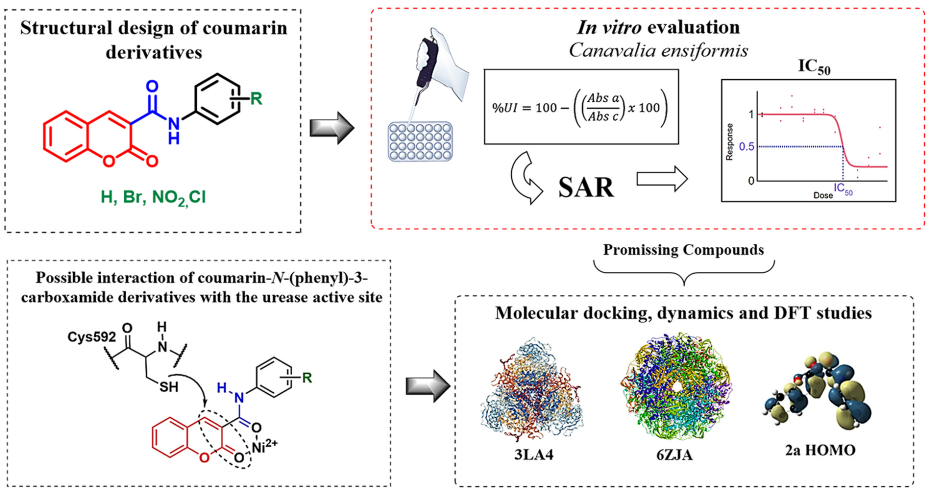

Figure 1. Structural design, experimental, and *in silico* approaches were applied to evaluate *N*-(R-phenyl)-3-carboxamide-coumarin derivatives as potential urease inhibitors (**2a-2j**).

Synthesis of *N*-phenyl-3-carboxamide-coumarin derivatives (**2a-2j**)

Derivatives **2a-2j** were synthesized using the method described by Bispo *et al.*,[16] with modifications. Firstly, coumarin-3-carboxylic acid (**1**, 0.792 mmol) was suspended in 1.20 mL of thionyl chloride ($SOCl_2$, 20 eq.). This mixture was heated under reflux for 2 h 30 min. Then, the $SOCl_2$ excess was removed under reduced pressure, and in the chloride *in situ* produced, a solution of the corresponding aniline (0.792 mmol, 1.0 eq) in 10 mL of dry acetone was added into the flask. The reaction remained under reflux for 1 h. Subsequently, the solution was poured into crushed ice, and the precipitate was filtered under vacuum and washed with cold distilled water and ethyl ether (both 3 × 5 mL). Thus, derivatives **2a-2j** were obtained in 75-92% yields.

N-Phenyl-3-carboxamide-coumarin (**2a**)

Yellow solid; 89% yield; mp 266 °C; lit.[17] 253.5-255 °C; ^{1}H NMR (400.1 MHz, $CDCl_3$) δ 10.84 (1H, s, NH), 9.03 (1H, s, H4), 7.77-7.68 (4H, m, H5, H7, H15 and H17), 7.47-7.37 (4H, m, H6, H8, H14 and H18), 7.19-7.15 (1H, m, J_1 8.5, J_2 1.0 Hz, H16);[17] HSQC (400.1/100.6 MHz, DMSO-d_6) δ 8.93→147.8 (H4→C4), 8.0-8.02→130.84 (H8→C8), 7.77-7.80→134.7 (H7→C7), 7.72-7.74→120.4 (H5→C5), 7.55-7.57→116.8 (H15/H17→C15/C17), 7.46-7.49→125.7 (H6→C6), 7.38-7.41→128.48 (H14/H18→C14/C18), 7.14-7.17→124.7 (H16/C16); MS *m/z*, 265 (9%), 173 (100%).

N-(2-Bromophenyl)-3-carboxamide-coumarin (**2b**)

White solid; 88% yield; mp 236 °C; lit.[18] 218-219 °C; ^{1}H NMR (400.1 MHz, $CDCl_3$) δ 11.23 (1H, s, NH), 9.02 (1H, s, H4), 8.52 (1H, dd, J_1 8.3, J_2 1.5 Hz, H15), 7.77-7.68 (2H, m, H5 and H7), 7.61 (1H, dd, J_1 8.0, J_2 1.4 Hz, H18), 7.4-7.33 (3H, m, H6, H8 and H17), 7.06-7.01 (1H, m, H16);[18] HSQC (400.1/100.6 MHz, DMSO-d_6) δ 9.11→149.6 (H4→C4), 8.46-8.48→122.8 (H15→C15), 8.07-8.09→131.1 (H8→C8), 7.79-7.83→135.3 (H5→C5), 7.72-7.74→133.3 (H7→C7), 7.57-7.58→116.7 (H18→C18), 7.47-7.51→125.8 (H6→C6), 7.44-7.48→128.9 (H17→C17), 7.11-7.15→126.6 (H16→C16); MS *m/z*, 264 (21%), 173 (67%), 89 (100%).

N-(3-Bromophenyl)-3-carboxamide-coumarin (**2c**)

Yellow solid; 92% yield; mp 246 °C; lit.[18] 232-233 °C; ^{1}H NMR (400.1 MHz, $CDCl_3$) δ 10.89 (1H, s, NH), 9.02 (1H, s, H4), 8.04 (1H, t, J_1 1.9 Hz, H14), 7.78-7.69 (2H, m, H5 and H7), 7.62 (1H, ddd, J_1 8.0, J_2 1.9, J_3 1.2 Hz, H18), 7.49-7.40 (2H, m, H6 and H8), 7.32-7.28 (1H, m, H16), 7.23 (1H, d, J_1 8.0 Hz, H17);[18] HSQC (400.1/100.6 MHz, DMSO-d_6) δ 8.90→147.9 (H4→C4), 8.11→122.7 (H14→C14), 8.00-8.02→130.9 (H16→C16), 7.77-7.80→134.9 (H8→C8), 7.55-7.56→116.8 (H5→C5), 7.62-7.64→119.4 (H7→C7), 7.46-7.49→125.9 (H6→C6), 7.34-7.35→127.7 (H17/C17), 7.34-7.35→134.5 (H18→C18); MS *m/z*, 343 (1%), 173 (100%), 89 (97%).

N-(4-Bromophenyl)-3-carboxamide-coumarin (**2d**)

Yellow solid; 83% yield; mp 268 °C; lit.[18] 247-248 °C; ^{1}H NMR (400.1 MHz, $CDCl_3$) δ 10.88 (1H, s, NH), 9.02 (1H, s, H4), 7.77-7.69 (2H, m, H5 and H7), 7.68-7.63 (1H, m, H15 and H17), 7.52-7.48 (2H, m, H14 and H18), 7.48-7.40 (2H, m, H6 and H8);[18] HSQC (400.1/100.6 MHz, DMSO-d_6) δ 8.91→147.9 (H4→C4), 8.00-8.02→130.7 (H15/H17→C15/C17), 7.77-7.80→134.8 (H8→C8), 7.71-7.73→122.3 (H5/H7→C5/C7), 7.56-7.58→132.4 (H14→C14), 7.54-7.56→132.4 (H18→C18), 7.46-7.49→126.0 (H6/H8→C6/C8); MS *m/z*, 343 (1%), 173 (96%), 89 (100%).

N-(2-Nitrophenyl)-3-carboxamide-coumarin (**2e**)

Yellow solid; 80% yield; mp 243 °C; lit.[19] 226-227 °C; ^{1}H NMR (400.1 MHz, $CDCl_3$) δ 12.56 (1H, s, NH), 9.00 (1H, s, H4), 8.75 (1H, dd, J_1 8.5, J_2 1.2 Hz, H15), 8.22 (1H, dd, J_1 8.4, J_2 1.4 Hz, H18), 7.77-7.65 (3H, m, H5, H7 and H17), 7.49-7.38 (2H, m, H6 and H8), 7.29 (1H, dd, J_1 8.4, J_2 1.1 Hz, H16);[19] HSQC (400.1/100.6 MHz, DMSO-d_6) δ 9.09→150.0 (H4→C4), 8.56-8.58→124.4 (H15→C15), 8.18-8.20→126.1 (H18→C18), 8.06-8.08→131.2 (H5→C5), 7.80-7.84→135.5 (H16/H17→C16/C17), 7.56-7.58→116.8 (H7→C7), 7.47-7.50→125.8 (H8→C8), 7.38-7.42→125.2 (H6→C6); MS *m/z*, 264 (11%), 173 (93%), 89 (100%).

N-(3-Nitrophenyl)-3-carboxamide-coumarin (**2f**)

White solid; 82% yield; mp 292 °C; ^{1}H NMR (400.1 MHz, $CDCl_3$) δ 11.14 (1H, s, NH), 9.06 (1H, s, H4), 8.73 (1H, t, J_1 2.1 Hz, H14), 8.01-8.05 (2H, m, H16 and H18), 7.80-7.72 (2H, m, H5 and H7), 7.57-7.51 (1H, dd, J_1 14.9, J_2 6.8 Hz, H17), 7.49-7.43 (2H, m, H6 and H8);[20] HSQC (400.1/100.6 MHz, DMSO-d_6) δ 8.93→148.2 (H4→C4), 8.81→114.7 (H14→C14), 8.05→126.7 (H16→C16), 8.02→119.5 (H17→C17), 8.01→130.8 (H18→C18), 7.78-7.71→134.9 (H5→C5), 7.77-7.70→130.9 (H7→C7), 7.56-7.58→116.8 (H8→C8), 7.47-7.50→125.7 (H6→C6); MS *m/z*, 310 (2%), 173 (100%), 89 (84%).

N-(4-Nitrophenyl)-3-carboxamide-coumarin (**2g**)

White solid; 79% yield; mp 366 °C; ^{1}H NMR (400.1 MHz, $CDCl_3$) δ 11.27 (1H, s, NH), 9.05 (1H, s, H4), 8.28 (2H, d, J_1 9.1 Hz, H15 and H17), 7.94 (2H, d, J_1 9.0 Hz, H14 and H18), 7.80-7.73 (2H, m, H5 and H7), 7.52-7.44 (2H, m, H6 and H8);[20] HSQC (400.1/100.6 MHz, DMSO-d_6) δ 8.93→148.2 (H4→C4), 8.28-8.30→125.6 (H15/H17→C15/C17), 8.03→130.92 (H14→C14), 8.01-7.99→120.43 (H18→C18), 7.78-7.82→135.1 (H5/H7→C5/C7), 7.56-7.58→116.9 (H6→C6), 7.47-7.50→126.0 (H8→C8); MS *m/z*, 310 (3%), 173 (100%), 89 (84%).

N-(2-Chlorophenyl)-3-carboxamide-coumarin (**2h**)

White solid; 92% yield; mp 238 °C, lit.[18] 220-221 °C; ^{1}H NMR (400.1 MHz, $CDCl_3$) δ 11.34 (1H, s, NH), 9.02 (1H, s, H4), 8.56 (1H, dd, J_1 8.2, J_2 1.0 Hz, H15), 7.77-7.68 (2H, m, H5 and H7), 7.49-7.39 (3H, m, H6, H8 and H17), 7.33 (1H, m, H18), 7.14-7.07 (1H, m, H16);[18] HSQC (400.1/100.6 MHz, DMSO-d_6) δ 9.10→149.5 (H4→C4), 8.52-8.54→122.2 (H15→C15), 8.09-8.07→131.1 (H18→C18), 7.80-7.83→135.3 (H17→C17), 7.57-7.59→116.8 (H7→C7), 7.57-7.59→129.90 (H5→C5), 7.51-7.48→125.9 (H6→C6), 7.44-7.40→128.3 (H8→C8); MS *m/z*, 299 (5.3%), 173 (100%), 264 (61%).

N-(3-Chlorophenyl)-3-carboxamide-coumarin (**2i**)

Yellow solid; 84% yield; mp 248 °C, lit.[18] 217-218 °C; ^{1}H NMR (400.1 MHz, $CDCl_3$) δ 10.90 (1H, s, NH), 9.02 (1H, s, H4), 7.90 (1H, t, J_1 1.8 Hz, H14), 7.78-7.69 (2H, m, H5 and H7), 7.56 (1H, dd, J_1 8.2, J_2 1.0 Hz, H18), 7.47-7.41 (2H, dd, J_1 16.3, J_2 8.4 Hz, H6 and H8), 7.30 (1H, t, J_1 8.2 Hz, H16), 7.14 (1H, dd, J_1 8.0, J_1 0.9 Hz, H17);[18] HSQC (400.1/100.6 MHz, DMSO-d_6) δ 8.91→148.0 (H4→C4), 8.00-8.03→130.9 (H14→C14), 7.98→119.9 (H16→C16), 7.77-7.81→134.9 (H17→C17), 7.58-7.59→118.9 (H18→C18), 7.55-7.57→116.8 (H5→C5), 7.46-7.49→125.8 (H7→C7), 7.42→131.2 (H8→C8), 7.20-7.23→124.6 (H6→C6); MS *m/z*, 299 (14%), 173 (100%), 89 (34%).

N-(4-Chlorophenyl)-3-carboxamide-coumarin (**2j**)

Yellow solid; 75% yield; mp 260 °C; lit.[18] 264-265 °C; ^{1}H NMR (400.1 MHz, $CDCl_3$) δ 10.88 (1H, s, NH), 9.02 (1H, s, H4), 7.76-7.69 (4H, m, H5, H7, H15 and H17), 7.47-7.41 (2H, dd, J_1 16.2, J_2 8.2 Hz, H6 and H8), 7.34 (2H, d, J_1 8.8 Hz, H14 and H18);[18] HSQC (400.1/100.6 MHz, DMSO-d_6) δ 8.91→147.9 (H4→C4), 7.80→134.7 (H14→C14), 7.79-7.76→122.0 (H15/H17→C15/C17), 7.57-7.55→116.7 (H18→C18), 7.49-7.46→125.8 (H5/H7→C5/C7), 7.46-7.44→129.3 (H6/H8→C6/C8). MS *m/z* 299 (16%), 173 (100%), 89 (32%).

Urease inhibition assay and determination of half of the maximum inhibitory concentration (IC_{50})

The urease inhibition screening was performed as described by our research group.[21] In 96-well plates, the reaction mixture was prepared by addition of 55 µL phosphate buffer solution (100 mM, 7.4 pH) with 1 mM ethylenediaminetetraacetic acid (EDTA), 100 µL of the substrate (10 mM urea), 25 µL of CEU type III (Sigma-Aldrich, Saint Louis, USA) enzyme solution (0.035 mM) and 10 µL of test compound (0.5 mM). After incubation for 30 min at 45 °C, the reaction was cooled down for 10 min. Sequentially, 40 µL of phenol reagent (a mixture of 1% phenol and 0.05% of sodium nitroprusside) and 40 µL of alkaline reagents (0.5% NaOH and 0.1% sodium hypochlorite) were added to each of the wells. After 20 min, the final absorbance of the reaction mixture was recorded at 630 nm using a microplate reader (Synergy HT, BioTek-Agilent, Santa Clara, USA). Urease inhibition (I) was calculated after measuring absorbance values using the equation 1.

$$I(\%) = 100 - \left(\left(\frac{\text{Abs a}}{\text{Abs c}} \right) \times 100 \right) \quad (1)$$

where Abs a is the observed absorbance for the samples, and Abs c is the observed absorbance for the control. Thiourea was used as a reference to urease inhibitors.

For the determination of the half-maximal inhibitory concentration (IC_{50}), compounds **2b**, **2d**, and **2e** were evaluated in different concentrations (5, 10, 20, 30, and 50 µM) using the same protocol described above. The assay was performed in triplicate, and IC_{50} values were calculated by nonlinear regression using GraphPad Prism 8.0.2.[22] Statistical analyses were performed using SISVAR software (version 5.70).[23] Distinct letters indicate a significant difference between treatments by Scott-Knott ($P < 0.05$) test.

Molecular modeling studies

DFT calculations

The DFT calculations were performed with the Gaussian 09 package[24] using the functional B3LYP exchange-correlation hybrid[25,26] and the 6-311G(d,p) basis-set.[27,28] The Polarized Continuum Model (PCM, solvent = water) also was adopted, in agreement with other studies involving molecules with biological activity.[29]

Protein and ligands preparation for molecular docking study

The X-ray crystal structure of CEU (PDB ID: 3LA4 resolution: 2.05 Å[30]) and HPU (PDB ID: 6ZJA, resolution: 2.00 Å[31]) was obtained from the Protein Data Bank.[30] All ions (except the Ni^{II} ions) and waters were removed. To the 3LA4 structure, the KCX490 (Lys490), CME59 (Cys59), CME207 (Cys207), and CME592 (Cys592) were modified since the molecular docking programs did not recognize these residues. To 6ZJA, the B subunit was considered since there is active binding. The center of the binding site to both enzymes was considered the middle between the Ni^{II} ions: CEU defined as X = –39.959, Y = –44.679, and Z = 74.986; HPU defined as X = 231.5970, Y = 239.1290, and Z = 195.9730. The 2D structures of **2b**, **2d**, and **2e** were constructed using ChemDraw,[32] and 3D structures were constructed in the Discovery Studio Visualizer program (v.19.1.0.18287),[33] followed by geometry optimization using the MMFF94 force field implemented in the Avogadro program (v. 1.2.0).[34]

Molecular docking procedure

To CEU, a consensus molecular docking study was performed using AutoDock[35] AutoDock Vina[36] and GOLD.[37] The AutoDock Tools interface (v 1.5.6) was used for protein and ligand preparation for the molecular docking study with AutoDock 4.2 and AutoDock Vina software. After adding the polar hydrogen atoms, the Kollman and Gasteiger charge methods were applied to the protein and ligand. The grid box dimension considered was 60 × 60 × 60 $Å^3$ with a grid spacing of 0.375 Å for AutoDock 4.2 and 30 × 30 × 30 $Å^3$ with a grid spacing of 1 Å for AutoDock Vina. The additional parameters were considered as default. The Genetic Algorithm (GA) and the Lamarckian Genetic Algorithm (LGA) scoring functions were implemented in AutoDock 4.2, and the Vina scoring function was implemented in AutoDock Vina carried out with 10 interactive runs. Then, the lowest energy conformation was used for docking analysis.

The consensus molecular docking using the GOLD program (v. 2020.1) was performed to CEU considering the following scoring functions: GoldScore,[37] ChemScore,[38] ChemPLP,[39] and Astex Statistical Potential (ASP).[40] About HPU, the molecular docking was validated by redocking procedure considering the crystallized ligand (PDB ID: DJM), using the scoring function ASP. For both enzymes CEU and HPU, the hydrogen atoms were added to the protein supported on ionization inferred by the software, considering pH = 7, the number of genetic operations, and another parameter was set as default in each run. The binding site was defined within a 10 Å radius to CEU and 15 Å to HPU, with the ligands subjected to 50 interactive runs. The highest score was used to determine the best conformation for docking analysis. The poses resulting from the molecular docking studies were selected from the root-mean-square deviation (RMSD) values < 2.0 Å, and the analysis of the intermolecular interactions were carried out using the Discovery Studio Visualizer program (v.19.1.0.18287),[33] and figures were built in the Pymol program (version 3.8).[41]

Molecular dynamics simulation

The poses obtained in the docking studies were used for molecular dynamics simulations with the CHARMM36 force field[42] employing the GROMACS program.[43] The ligands parameters were generated through the Cgenff server.[44,45] To CEU and HPU targets, the protonation states were determined using the H^{++} server,[46,47] considering the pH 7.4 and 8.0, respectively. After that, the protein topology was obtained using the pdb2gmx module. Each protein-ligand system was inserted and centered in a triclinic box (dimensions: 10.772 × 7.312 × 7.653 nm; volume: 602.79 nm^3) with periodic conditions. The water model considered was TIP3P,[48] and the complex (target-ligand-water) was neutralized with 19 atoms of Na^+ ions. The energy minimization, equilibration, and production steps were executed according to our previous work.[49,50] The energy minimization step was realized using the steepest-descent algorithm followed by the gradient conjugate algorithm with a convergence criterion of 1000 and 100 kJ mol^{-1} nm^{-1}, respectively. Next, the equilibration step was realized considering 300 K and 1 bar with position restraint to the whole system, except for ions and water molecules. In the first step (1 ns), the NVT (constant-volume ensemble) ensemble was considered constant, and in the second step (1 ns), the system was viewed as isothermal-isobaric (NPT ensemble). The above equilibration allows the system to reach atom speeds compatible with the target temperature and pressure. Furthermore, the position restraint of the protein-ligand atoms allows ions and water molecules to organize optimally along the protein surface, forming more structured solvation layers. Temperature control was achieved with the V-rescale thermostat[51] and pressure control through the Parrinello-Rahman barostat.[52] All bonds to hydrogen atoms in the complex were constrained using the linear constrained solver (LINCS) algorithm.[53] The long-distance electrostatic interactions were treated using the Particle-Mesh Ewald (PME) algorithm[54] and the cut-off radius applied to the van der Waals and Coulomb interactions was 1 nm. After equilibration, molecular dynamics (MD) simulations were carried out during 100 ns, considering the NPT ensemble without any position restraint, using 2 fs integration time and 10 Å of cut-off radius to the long-distance interactions.

MD simulation analysis

All complexes were evaluated regarding RMSD, RMSF (root-mean-square fluctuation), and hydrogen bonds (cutoff radius of 4.0 Å and cutoff angle of 30 Å). We used the HbMap2Grace software[55] to calculate the frequency of the hydrogen bonds and the VMD software[56] to visualize the trajectories of the simulations. RMSD, RMSF, and hydrogen bonds were plotted with the xmgrace tool.[57] The binding free energies (ΔG_{bind}) were calculated using the modified method of molecular mechanics Poisson-Boltzmann surface area (MMPBSA) through the module added to GROMACS 5.1.4 program package.[58]

Results and Discussion

The synthesis of the series of ten *N*-(R-phenyl)-3-carboxamide-coumarin derivatives (**2a-2j**) was efficiently reproduced according to Figure 2. Firstly, coumarin-3-carboxylic acid (**1**) was prepared through a Knovenagel condensation between 2-hydroxybenzaldehyde with Meldrum's acid, using water as a solvent.[15] Then, acid **1** was converted *in situ* into the corresponding acyl[16] and condensate with the corresponding aniline (R-C_6H_4-NH_2), leading to the *N*-(R-phenyl)-3-carboxamide-coumarin derivatives (**2a-2j**) in 75-92% yields (Figure 2).

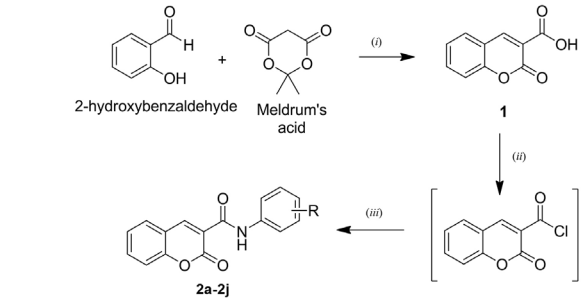

Figure 2. Reagents and conditions for the synthesis of *N*-(R-phenyl)-3-carboxamide-coumarin derivatives (**2a-2j**): (*i*) H_2O, 75 °C, 4 h, 92%; (*ii*) $SOCl_2$ (20 eq), reflux, 2 h 30 min; (*iii*) corresponding aniline (R-C_6H_4-NH_2), acetone, reflux, 1 h, 75-92%.

All the *N*-(R-phenyl)-3-carboxamide-coumarin structures (**2a-2j**) were confirmed by spectral data, which agree with previous data reported.[17-19] Since the compounds are already described in the literature and are poorly soluble in common deuterated solvents, we characterized them by mass spectroscopy, ^{1}H NMR, and heteronuclear single quantum correlation (HSQC) experiments.

The mass spectra showed the molecular ion peaks with the *m/z* ratio compatible with the substances molar mass (MM), ranging from 265 to 344 g mol^{-1}. Besides, ^{1}H NMR spectra showed characteristic signals of the amides **2a-2j**, such as broad singlets at 10.84-12.56 ppm relative to the NH proton and the singlet at 9.06-9.00 ppm corresponding to H4 of the coumarin ring. Moreover, the benzoyl group was confirmed by the expected signals for its aromatic protons between 8.75 and 7.01 ppm. The HSQC spectra generally showed the characteristic carbon signals from aromatic rings between 116 at 130 ppm and CH from the Michael acceptor group between 134 at 149 ppm (Figures S1-S35, Supplementary Information (SI) section).

All ten compounds (**2a-2j**) were assayed against CEU *in vitro* using the colorimetric indophenol method.[59] The results of the *in vitro* screening of **2a-2j** (0.5 mM) against the enzyme are shown in Table 1 and were expressed as a percentage of urease inhibition (I), using thiourea as a standard inhibitor. Besides, the IC_{50} values were determined for derivatives with a urease inhibition above 60% (Table 1).

Table 1. *In vitro* inhibitory activity against jack bean (*Canavalia ensiformis*) urease of coumarin derivatives **2a-2j**, in reactions containing 10 mM urea, expressed as the percentage of urease inhibition (I) and the half-maximal inhibitory concentration (IC_{50})

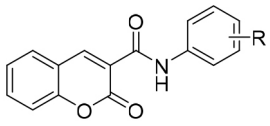

2a-2j

Compound	R	I / %	IC_{50} / μM
2a	H	55.97 ± 4.98[a]	Nd
2b	2-Br	**64.18 ± 0.00[b]**	**35.29 ± 3.86[e]**
2c	3-Br	59.17 ± 1.65[a]	Nd
2d	4-Br	**65.24 ± 0.60[b]**	**22.86 ± 4.84[e]**
2e	2-NO_2	60.23 ± 0.76[a]	Nd
2f	3-NO_2	56.18 ± 3.17[a]	Nd
2g	4-NO_2	56.29 ± 5.43[a]	Nd
2h	2-Cl	59.27 ± 0.30[a]	Nd
2i	3-Cl	47.65 ± 2.86[c]	Nd
2j	4-Cl	42.43 ± 1.81[c]	Nd
Thiourea	–	**88.59 ± 0.45[d]**	**28.89 ± 1.52[e]**

I: percentage of urease inhibition (%I) ± SEM (standard error of the mean, n = 2); IC_{50}: half maximal inhibitory concentration ± SEM (n = 2); Nd: not determined; Different letters indicate statistical difference by Scott-Knott test ($P < 0.05$). In bold are highlighted the best compounds of the series.

The *in vitro* screening results showed that all derivatives are potential urease inhibitors, with an inhibitory percentage ranging from 42 to 65%. In addition, a preliminary SAR study based on the I indicated that compounds presenting bromo at *ortho* (**2b**) and *para* (**2d**) positions showed the highest I when compared to *meta* (**2c**) position, suggesting

that stereo and/or electronic effects could influence on the inhibitory activity. Besides, all bromine derivatives (**2b-2d**) have better I than the corresponding nitro (**2e-2g**) and chloro (**2h-2i**) derivatives at the same position in the ring. However, nitro-substituted compounds (**2e-2g**) and **2h** (R = 2-Cl) presented around 60% of urease inhibition, indicating that the presence of chloro at *meta* (**2i**) and *para* (**2j**) positions seemed to be prejudicial to the inhibitory effect since the values observed were around 47%.

The IC_{50} was determined for the best compounds **2b** and **2d** (I = 65%), presenting values of approximately 35 and 23 μM, respectively. In addition, these compounds did not show a significant statistical difference compared to standard inhibitor thiourea, showing that the coumarin class can be considered a promising scaffold for developing urease inhibitors.

Quantum calculations were used to evaluate the electronic structure of compounds **2a**, **2b**, and **2d**. The graphical representation of the frontier molecular orbitals highest occupied molecular orbital (HOMO) and lowest unoccupied molecular orbital (LUMO) in Figure 3 showed that in **2a**, HOMO is delocalized by the complete molecular structure while LUMO was localized in coumarin-nucleus. The addition of the Br-group kept the LUMO localized in the coumarin-nucleus region while making the HOMO localized in the region of the phenyl-group, independent of the position of the substituent. These results show that the smaller electron-withdrawing nature of the substituent (Br-group) localized the frontier orbitals in different molecule regions.

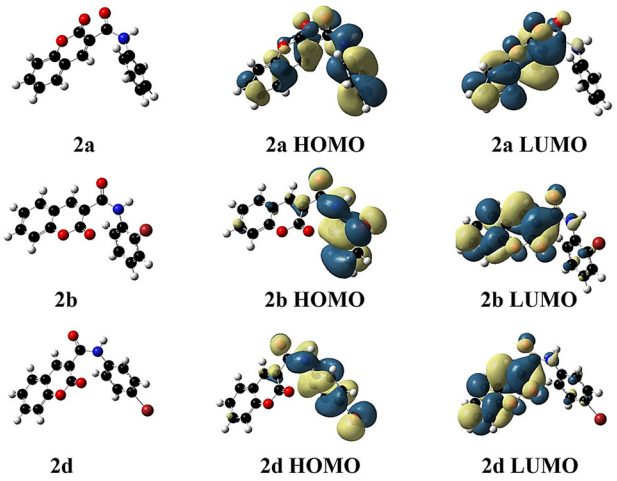

Figure 3. Graphical representation of **2a**, **2b**, and **2d**. The color difference is related to the signal of the wave function. Atoms: carbon (black), hydrogen (white), oxygen (red), nitrogen (blue), and bromine (brown).

The energies of frontier molecular orbitals can indicate tendencies in the abilities to withdraw and donating-electron. For example, the high energy of the HOMO indicates the excellent ability of the molecule to donate electrons, and the low energy of the LUMO indicates its ability to receive electrons.[60]

Comparing the results of the Br-substituent in distinct positions (Table 2), the presence of the Br in the 4-position increased the E_{HOMO}, suggesting the improvement of the coordination ability of the Ni. In the case of the LUMO, the position of the Br-group did not significantly change the energy of this orbital. In general, the increase in E_{HOMO} and the decrease in the E_{LUMO} caused by the Br-group in the 4-position improve the coordination abilities of Ni and suffer a nucleophilic attack on carbon B (C9, Figure S2, and Table S1, SI section) in comparison to **2a** and **2b**.

Table 2. Energies of the frontier molecular orbitals calculated with the theory level B3LYP/6-311G/PCM (solvent = water) compared with IC_{50} obtained

R	IC_{50} / μM	E_{HOMO} / eV	E_{LUMO} / eV	Gap / eV
H	Nd	–6.68	–2.34	4.34
2Br	35.29	–6.72	–2.51	4.21
4Br	22.86	–6.54	–2.49	4.05

IC_{50}: half maximal inhibitory concentration; Nd: not determined.

The gap value is a difference between the energies of LUMO and HOMO, and is an index of chemical reactivity: a smaller gap indicates high reactivity and low kinetic stability.[61] For **2a**, **2b**, and **2d**, it was observed that the addition of the Br-group and their change to the 4-position (compared to the 2-position) decreased the gap value. These results indicate that the position of the Br-group in the 4-position makes the coumarin-derivative more reactive.

The participation percentage of every atom on the HOMO and LUMO of **2a**, **2b**, and **2d** was calculated (Table S1). The results of the HOMOs showed that, for all three molecules, the atoms with a significant tendency to coordinate the Ni of the active site were O18 and N19 (Figure S2, SI section), with a contribution of around 5.00-7.50 and 7.00-12.00% to generating this orbital, respectively, indicating that the coordination to the Ni should occur by these atoms.

The results of the LUMOs showed that, for all three molecules, the atoms with a significant tendency to suffer a nucleophilic attack from S-atom of cysteine residue were C9 (carbon β) and C12 (Figure S2), with a contribution of around 7.00-14.50 and 4.00-12.00% to generating this orbital, respectively. Once C9 (carbon β) would be the atom that should react with a cysteine residue, high participation of this atom on LUMO was expected. Instead, it was observed that the Br-group increased the involvement of C9 on LUMO. The results of frontier orbitals suggest that

the substituent group that favored the biological activity of the coumarin derivatives was the Br-group in the 4-position of the phenyl ring (**2d**).

To predict the potential binding modes of the two promising compounds (**2b** and **2d**), we performed molecular docking studies using 3D structures of the CEU (PDB ID: 3LA4, 2.05 Å resolution)[30] and HPU (PDB ID: 6ZJA, 2.00 Å resolution).[31] Although ureases from diverse microorganisms, such as fungal, bacterial, and plants, have different characteristics, such as the number of polypeptide chains, studies indicate that regardless of the urease source, they have the same ancestor and, thus, share an active site of high similarity.[62] Therefore, it is common to carry out *in vitro* studies with the CEU since it is the most commercially accessible.

The CEU 3LA4 did not contain a co-crystalized inhibitor. Therefore, considering the importance of the docking validation process and the reliability of the pose obtained in several studies, we choose to apply herein the consensus docking.[63-65] The RMSD between the different poses are shown in Figures 3 and 4 for compounds **2b** (R = 2-Br) and **2d** (R = 4-Br), respectively.

By overlapping the structures of **2b** (R = 2-Br) shown in Figure 4a, we can see the similarity between the conformations obtained by LGA and GA scoring functions, confirmed by the RMSD value of 0.47 Å. Besides, the RMSD (Figure 4b) shows that there is also a consensus between the poses generated by ASP and ChemPLP, with an RMSD of 1.49 Å. Among the consensual amino acid residues, for GA and LGA, Arg439 and Ala436 stand out, responsible for the hydrogen bond with the oxygen atoms of the lactone in the coumarin ring, as well as the Ala440, Met558, Cys592 (flap), Gln635, Ala636 and Met637 residues that interact hydrophobically with the aromatic rings of derivative **2b** (Figure 4c). Besides, the distance (4.92 Å) between the thiol group of the Cys592 residue with the β carbon, Michael acceptor group of coumarin, does not allow the nucleophilic attack from the thiol group. Figure 4d reveals the consensual residues for the poses generated by ASP and ChemPLP. The compound only performed hydrophobic interactions in this case, with Ala436, Arg439, Ala440, His492, Asp494, His519, Cys592, His593, His594, Arg609, and Ala636 residues.

Figure 5a shows that compound **2d** (R = 4-Br) displays similar poses generated in at least three scoring functions. This result is confirmed by the analysis of the RMSD (Figure 5b), in which LGA, GA, and ChemPLP are consensual, with RMSD between poses below 1.2 Å. Also, ASP and ChemScore demonstrate RMSD < 2.0 Å, but the

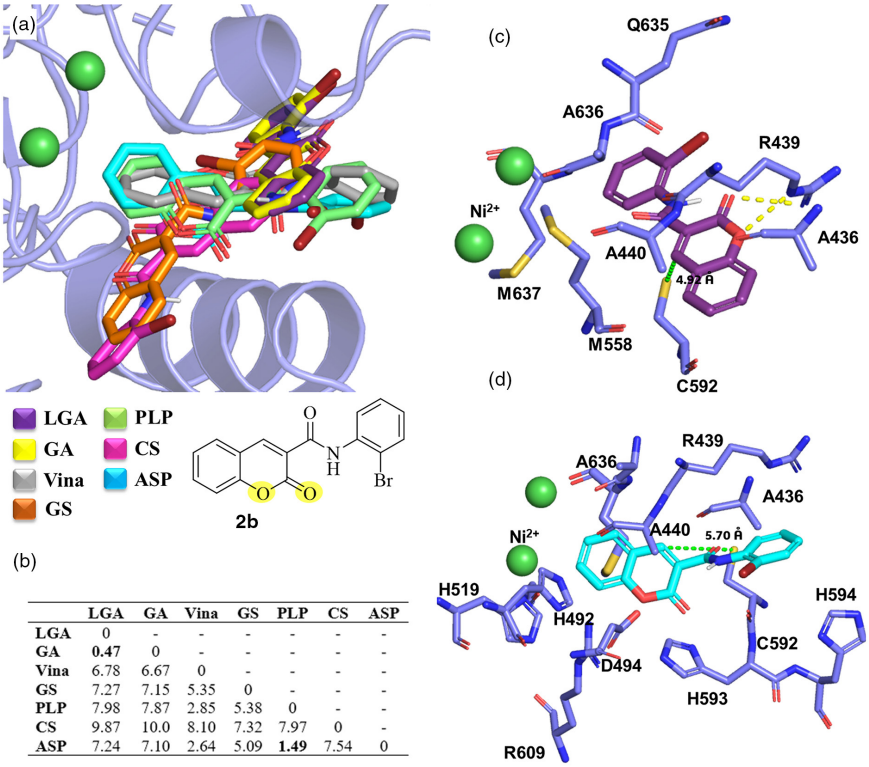

	LGA	GA	Vina	GS	PLP	CS	ASP
LGA	0	-	-	-	-	-	-
GA	**0.47**	0	-	-	-	-	-
Vina	6.78	6.67	0	-	-	-	-
GS	7.27	7.15	5.35	0	-	-	-
PLP	7.98	7.87	2.85	5.38	0	-	-
CS	9.87	10.0	8.10	7.32	7.97	0	-
ASP	7.24	7.10	2.64	5.09	**1.49**	7.54	0

Figure 4. (a) Overlapping conformations and (b) RMSD values obtained in molecular docking of compound **2b** (R = 2-Br) considering seven scoring functions (LGA, GA, Vina, GoldScore, ChemPLP, ChemScore, and ASP). Main interactions of **2b** with amino acid residues from consensus docking by the (c) LGA and GA and (d) ASP and ChemPLP scoring functions. The dashed yellow lines represent hydrogen bonds, and the green ones the distance between atoms. Atom colors: oxygen (red); nitrogen (blue); sulfur (yellow); hydrogen (white), nickel (green).

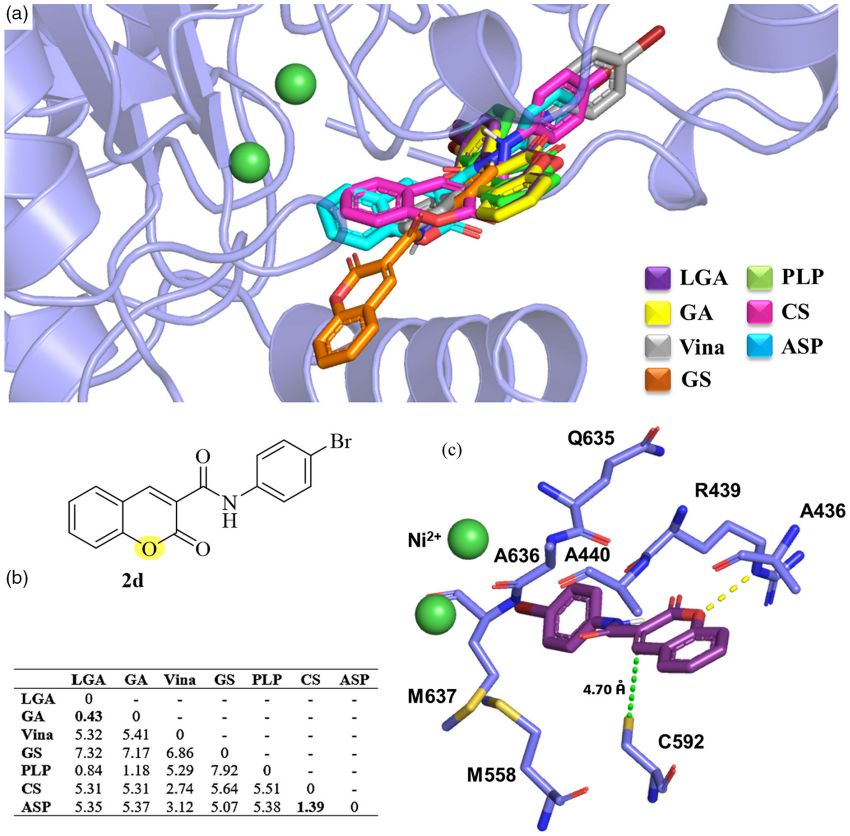

	LGA	GA	Vina	GS	PLP	CS	ASP
LGA	0	-	-	-	-	-	-
GA	**0.43**	0	-	-	-	-	-
Vina	5.32	5.41	0	-	-	-	-
GS	7.32	7.17	6.86	0	-	-	-
PLP	0.84	1.18	5.29	7.92	0	-	-
CS	5.31	5.31	2.74	5.64	5.51	0	-
ASP	5.35	5.37	3.12	5.07	5.38	**1.39**	0

Figure 5. (a) Overlapping conformations and (b) RMSD values obtained in molecular docking of compound **2d** (R = 4-Br) considering seven scoring functions (LGA, GA, Vina, GoldScore, ChemPLP, ChemScore, and ASP). (c) Main interactions of **2d** with amino acid residues from consensus docking by the LGA, GA, and ChemPLP scoring functions. The dashed yellow lines represent hydrogen bonds, and the green ones the distance between atoms. Atom colors: oxygen (red); nitrogen (blue); sulfur (yellow); hydrogen (white), nickel (green).

better consensus obtained was among the first highlighted poses. Figure 5c illustrates the main consensual interactions for compound **2d**. We emphasize the hydrogen interaction of Arg439 with the oxygen atom of the coumarin ring, while the other highlighted amino acids Ala436, Ala440, Met588, Cys592, and Asn635, Ala636 and Met637 perform hydrophobic interactions with the derivative. As noted for the **2b** derivative, the thiol group of Cys592 is located at 4.70 Å from the carbon β of coumarin of compound **2d**, making it difficult for the coumarin to suffer a nucleophilic attack from the group.

Overall, these results indicate a consensus for the two compounds between LGA and GA function scoring, with RMSD < 1.0 Å. It is interesting to note that due to the size of the evaluated molecules, the bis-coumarins assessed by Alomari *et al.*[11] have shown the same tendency discussed here since they do not reach the center of the enzyme active site, fitting only on the surface of the urease active site. Furthermore, we investigated the interactions by coumarins derivates **2b** and **2d** on active sites from bacterial HPU (6ZJA). The docking protocol to the ASP function score was successfully validated by redocking the presented RMSD value of 1.05 Å (Figure S1, SI section).

The compounds **2b** and **2d** demonstrated binding affinity to catalytic subunit B (Figure 6a). However, differently from what has been observed for CEU, the substituent position drastically altered the observed interactions since the compound **2b** was located on the surface of the protein in a region interacting with Met262, Glu292, Asn294, and Gly627 residues, far from the catalytic amino acids and nickel ions (Figure 6b). In contrast, the **2d** binding mode was observed close to the active site. In addition, one hydrogen bond between oxygen from the amide scaffold of **2b** was observed with His293 (Figure 6b). On the other hand, as mentioned for **2d**, the binding mode into the active site from HPU presented hydrophobic interactions mainly with His221 and His248, described by its coordination with Ni^{2+} ion; catalytic amino acids Asp362 and Met366; His322 at the top of the flap region,[31] and other residues as Gln142, Ala169, Glu222, Asp223, Phe334, and Ala365. In addition, one hydrogen bond between oxygen from the amide scaffold also was observed with Arg338 (Figure 6c).

We performed MD simulations with CEU and HPU-complexes of compounds **2b** and **2d** to complement data from molecular docking results. Initially, we investigated the RMSD profiles for both α-carbon atoms of the enzymes.

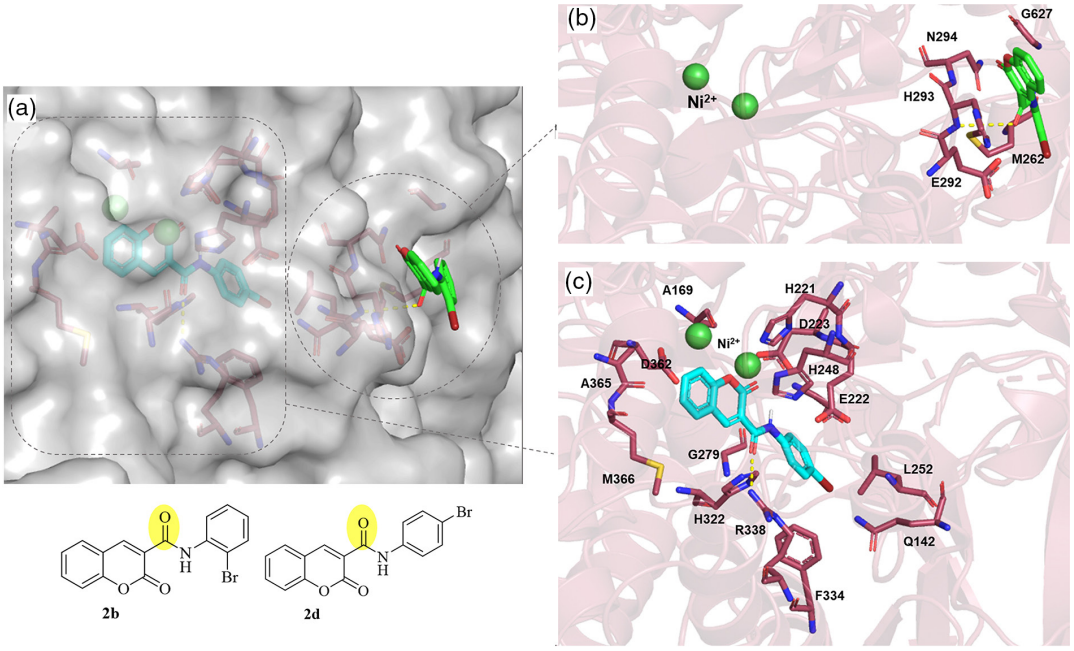

Figure 6. (a) Overlapping conformations of **2b** and **2d** coumarin derivatives in the catalytic subunit B of *H. pylori* urease 6ZJA. (b) Main interactions of **2b** (R = 2-Br) and (c) **2d** (R = 4-Br) with amino acid residues from molecular docking studies. Atom colors: oxygen (red); nitrogen (blue); sulfur (yellow); hydrogen (white), nickel (green).

The results of CEU suggested stability compared to the docking and similar behavior between complexes with values of 2.36 ± 0.27 and 2.32 ± 0.37 Å to CEU-**2b** and CEU-**2d**, respectively (Figure 7a). The same behavior was observed in HPU results, where the RMSD profiles values were 2.54 ± 0.22 and 3.29 ± 0.36 Å for HPU-**2b** and HPU-**2d** complexes, respectively (Figure 7b). In both targets, it is possible that the low standard deviation (SD) indicated α-carbon atoms were stable between the frames during the 100 ns simulation.[66,67]

We observed a displacement of **2d** from the active site in the first ten ns of the CEU simulations for the RMSD profile of ligands. However, it remained stable in another region with an RMSD value of 8.54 ± 1.30 Å and an SD greater

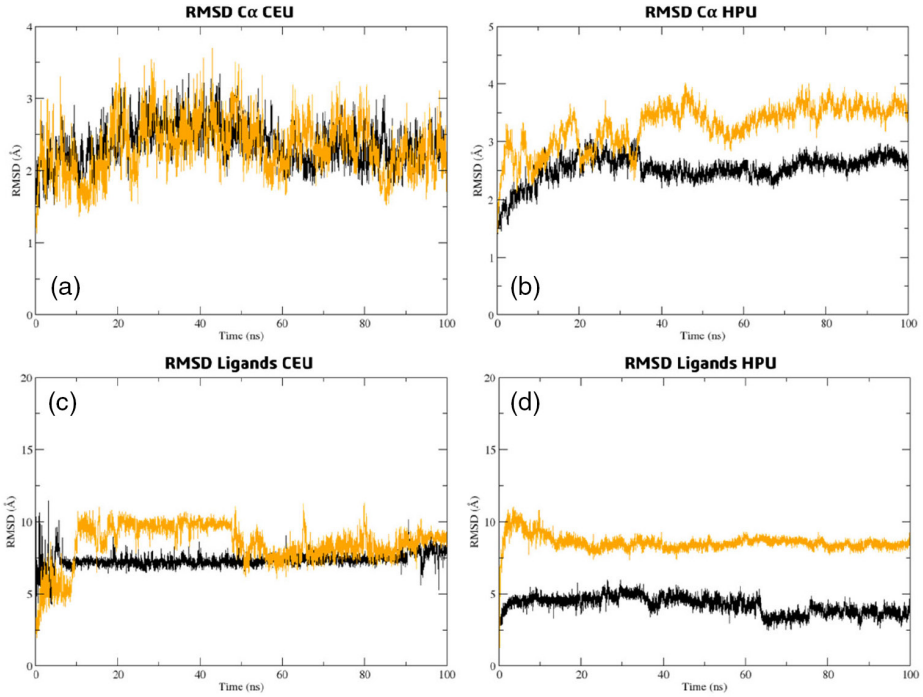

Figure 7. The RMSD analysis of (a) CEU and (b) HPU α-carbon atoms of the enzymes in the presence of the compounds **2b** (black) and **2d** (orange).

than 1.00 (Figure 7c). On the other hand, ligand **2b** showed stability from the beginning of the simulation with smaller SD values and an RMSD value of 7.32 ± 0.46 Å (Figure 7c). During the HPU simulations, we noticed distinct RMSD values among the ligands. Specifically, the RMSD value for **2d** (8.57 ± 0.45 Å) was twice as high as **2b** (4.22 ± 0.59 Å) but with a lower standard deviation. However, both ligands demonstrated stability from the initial nanoseconds of the MD simulations (Figure 7d).

In addition, the hydrogen bond analysis of the CEU and HPU complexes with compounds **2b** and **2d** were performed to understand structural changes and predict the binding mode with molecular targets. The examination for CEU complexes demonstrated direct hydrogen bonds of **2b** only with His594 with a short 9% lifetime, proving unable to reach the center of the active site of the enzyme (Figure 8a). Interestingly, during MD simulations, **2d** displayed a slightly longer lifetime for hydrogen-bond interactions with Ala636 (15.8%), Arg609 (9.6%), and His593 (7.1%) (Figure 8b). It is worth noting that the binding mode observed for **2d** in the MD simulations was in the internal region of the active site, as opposed to the docking pose. This displacement of the initial bind location was also confirmed by the RMSD calculation discussed previously.

During the analysis of HPU complexes, it was observed that there were intermittent hydrogen bonds between **2b** and amino acids His322 and Arg338 and short lifetime. Additionally, a stronger hydrogen bond with up to 55% lifetime was observed with Ala278, which lasted until the final stages of MD simulation (Figure 9a). The amino acids His332, Arg338, and Ala278 were on the HPU active site mobile flap. It is well-known that this flap strictly controls substrate entry and product exit from the urease active site.[68,69] These findings are according to the low RMSD value observed since the flap region is close to the active site of HPU. On the other hand, the RMSD value to the HPU-**2d** complex was twice more significant, and MD simulations revealed weak interactions with His274 responsible for Ni^{2+} coordination. In contrast, persistent interactions occurred with His314 (55%), showing movement from the surface into the active site (Figure 9b). Thus, continuous interaction with these residues could inhibit the urease.

The RMSF evaluated the residue mobility. We analyzed especially the residues that form the active site of both ureases, regions between 136-362 to HPU and 409-633 to CEU (Figure 10). Based on previous observations, the RMSF results showed significant fluctuations of around 3 Å in the amino acids within the CEU active site. These fluctuations are particularly noticeable between 593-606, where hydrogen bond interactions occurred. This suggests that the presence of **2b** and **2d** could potentially affect the stability of the enzyme (Figure 10a). Additionally, there was

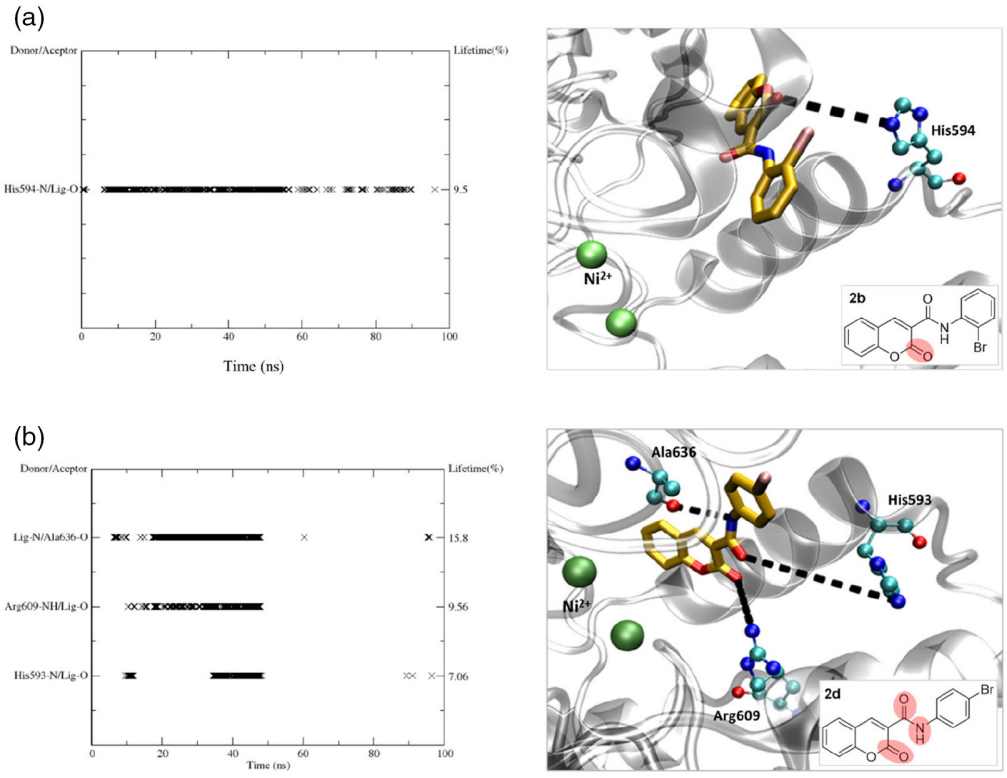

Figure 8. The predicted binding modes and the lifetime of compounds **2b** and **2d** hydrogen bonding interactions at the CEU active site during 100 ns MD. The red circles on 2D structures indicate which atoms involve amino acid bonds. Atom colors: oxygen (red); nitrogen (blue); bromine (salmon); nickel (green).

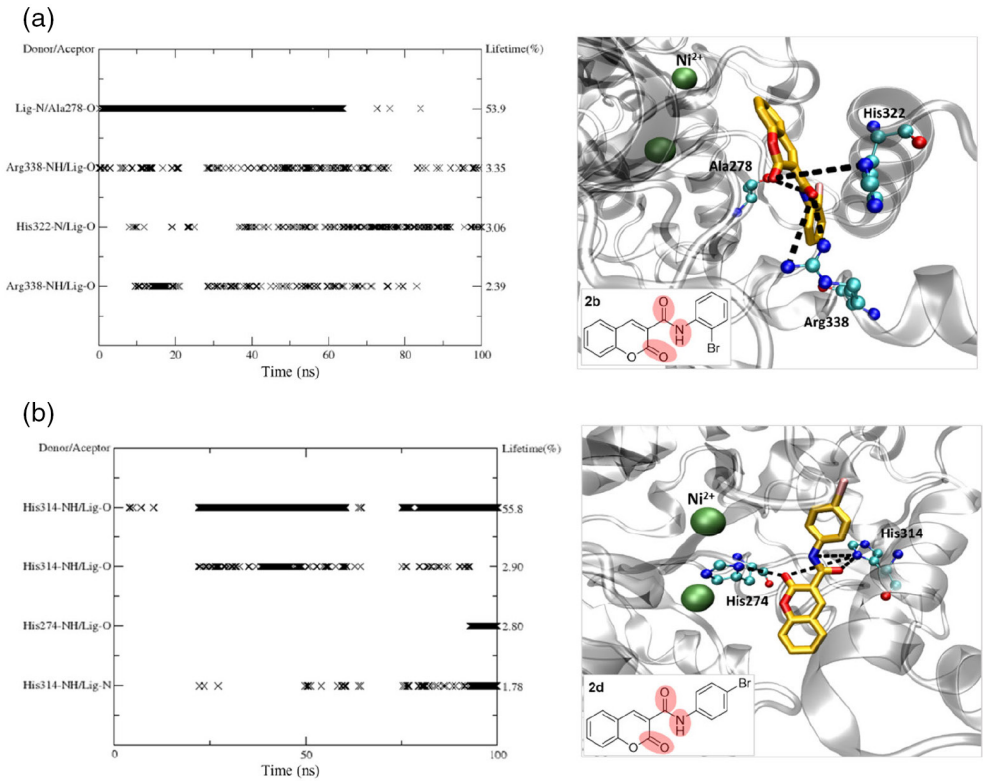

Figure 9. The predicted binding modes and the lifetime of compounds **2b** and **2d** hydrogen bonding interactions at the HPU active site during 100 ns MD. The red circles on 2D structures indicate which atoms involve amino acid bonds. Atom colors: oxygen (red); nitrogen (blue); bromine (salmon); nickel (green).

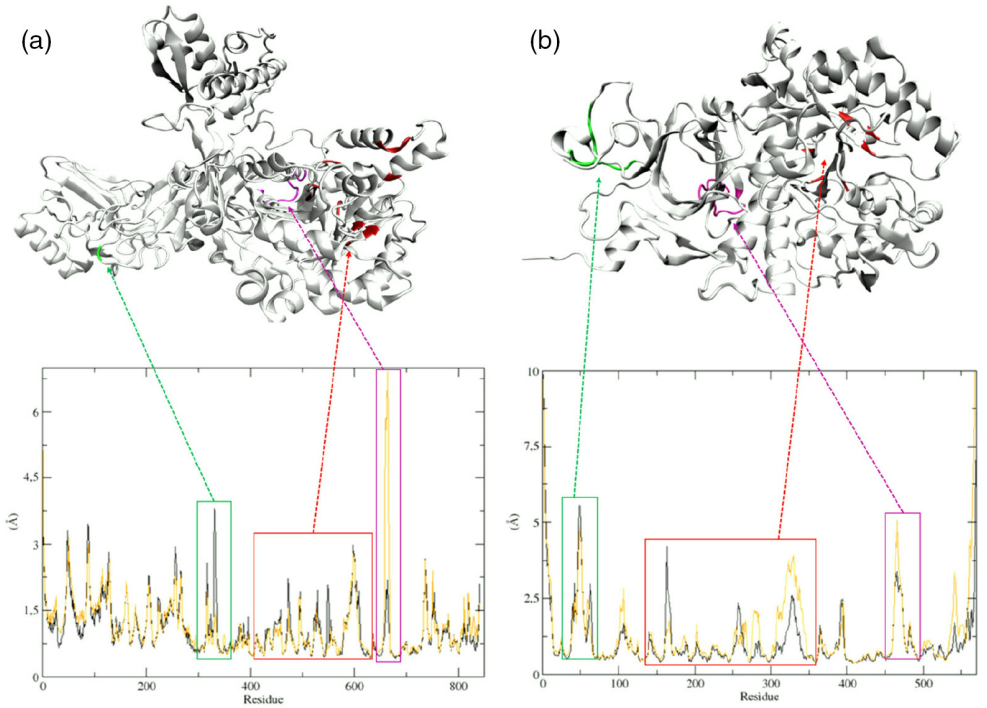

Figure 10. The RMSF analysis of (a) CEU and (b) HPU α-carbon atoms of the enzymes in the presence of the compounds **2b** (black) and **2d** (orange). The colored square in 3D structures indicates highlighted fluctuations of the active site (red) and flexible loops (green and pink).

considerable fluctuation in residues on flexible loops such as Pro332 (4 Å) due to **2b** binding and high fluctuation of 7 Å to Ser666 by **2d**. The HPU complexes displayed even higher fluctuations in the amino acids from the active site, with values ranging from 4 to 5 Å. This was observed for both **2b** and **2d** compounds, particularly in the region

of the mobile flap (residues 310-342), according to MD simulation findings (Figure 10b).

The ΔG_{bind} values were evaluated using the frames from the most representative cluster from the last 50 ns of the MD simulation. Compound **2d** had a better affinity than **2b** for both urease enzymes, presenting $\Delta G = -21.8$ kcal mol^{-1} to CEU-complex and $\Delta G = -12.1$ kcal mol^{-1} to HPU-complex (Table 3). The ΔG values for CEU-complexes are more representative (-15.9 and -21.8 kcal mol^{-1}) than HPU complexes (-7.08 and -12.1 kcal mol^{-1}), but this fact could be related to the active site characteristics of both enzymes. CEU has a smaller active site (106.95 Å^2) and can accommodate smaller ligands. On the other hand, HPU has a hydrophobic and more extensive active area (238.29 Å^2)[70] where larger substances such as these coumarin derivatives can interact more strongly.

The solvation energy analysis indicates a higher energy cost for ligands to enter the HPU active site due to its more hydrophobic environment than CEU.[71] Consequently, the entropic cost for ligands to access the site is elevated. Although our molecular dynamics study showed a tendency for the compounds to be more selective for HPU, the ΔG values were lower than for CEU. This is due to the energy values of van der Waals being compensated by the solvation energy, leading to a lower ΔG value for the HPU complexes (Table 3). As previously discussed, this is attributed to the hydrophobicity of the active site. In contrast, for CEU, the ligands tended to bind to the surface of the active site instead of entering the cavity, resulting in a relatively lower energetic cost of solvation and reflecting a higher ΔG observed (Table 3).

In summary, the results of molecular dynamics indicate that the amide and lactone scaffold were essential to the main interactions of both **2b** and **2d** compounds. The *para*-position of the bromine atom in the phenyl ring is believed to heighten the compounds affinity, which supports the DFT analyses. Moreover, the molecular dynamics study showed that these coumarin derivatives have a higher chance of selectivity by the bacterial enzyme than the vegetable one. The *in vitro* tests with CEU confirmed this observation, as derivatives **2b** and **2d** showed similar inhibition values. Our findings suggest that coumarins hold great potential for future enzymatic and phenotypic assays against *H. pylori*.

Conclusions

This research outlines a method for efficiently synthesizing ten *N*-(R-phenyl)-3-carboxamide-coumarin derivatives with high yields. All the compounds were effective inhibitors of CEU enzymatic activity *in vitro*. A study of structure-activity relationships by DFT discovered that the presence of bromo, particularly in the *ortho* and *para* positions, enhanced the compounds inhibitory activity. At the same time, a similar effect was not observed in the *meta* position. This finding was supported by molecular docking analysis, which indicated that the 4-Br substituent position is crucial for interacting with catalytic amino acids on the active site of both enzymes. Molecular dynamics simulations revealed that these coumarin derivatives may have selectivity for HPU, making them promising candidates for future enzymatic and phenotypic assays against *H. pylori*.

Supplementary Information

Supplementary information about DFT calculations and RMN spectra is free of charge at http://jbcs.sbq.org.br as PDF file.

Acknowledgments

This work was supported by the Coordenação de Aperfeiçoamento de Pessoal de Nível Superior Brasil (CAPES) under grant (number 001 and 88887.507109/2020-00) and Fundação de Amparo à Pesquisa do Estado do Rio de Janeiro (FAPERJ) (E-26/010.210.513/2019, E-26/205.966/2022, SEI-260003/009792/2021, SEI-260003/007043/2022 and SEI-260003/003788/2022). The authors wish to thank the Laboratory of Spectroscopy

Table 3. Binding free energy (mean ± standard deviation) of CEU and HPU-ligands complexes

Energy / (kcal mol^{-1})	CEU		HPU	
	Compound **2b**	Compound **2d**	Compound **2b**	Compound **2d**
ΔEvdw	–31.5 ± 1.67	–34.5 ± 2.49	–36.6 ± 1.21	–40.2 ± 2.27
ΔEelect	–0.53 ± 0.89	–2.39 ± 1.22	–3.99 ± 0.61	–7.87 ± 0.60
ΔEsolv	19.5 ± 4.38	18.4 ± 5.19	37.3 ± 4.42	40.0 ± 3.02
ΔEsasa	–3.35 ± 0.15	–3.36 ± 0.22	–3.82 ± 0.18	–4.06 ± 0.16
ΔG_{bind}	–15.9 ± 3.48	–21.8 ± 3.97	–7.08 ± 4.06	–12.1 ± 2.81

HPU: *Helicobacter pylori* ureases; CEU: *Canavalia ensiformis* ureases; ΔEvdw: Van der Walls energy; ΔEelect: eletrostatic energy; Esolv: solvatation energy; Esasa: SASA energy; ΔG_{bind}: binding free energy.

(ESPEC-UEL), Multiuser Laboratory of Nuclear Magnetic Resonance in Liquids (LABRMN-L/UFRJ), and Prof Dr Alviclér Magalhães for 2D-NMR analysis. Finally, the Centro Nacional de Processamento de Alto Desempenho em São Paulo (CENAPAD-SP) for the resources for the Molecular Dynamics simulations.

Author Contributions

Marciéli Fabris was responsible for conceptualization, methodology, formal analysis, investigation, writing; Priscila G. Camargo for methodology, formal analysis, investigation, writing; Mariana L. Silva for methodology, formal analysis; Talis U. Silva for methodology, formal analysis, research; Sérgio P. Machado for supervision, resources; Carlos R. Rodrigues for supervision, resources; Camilo H. S. Lima for supervision, software, review, and editing; Magaly G. Albuquerque for supervision, software, review, and editing; Marcelle L. F. Bispo for review, editing, project administration, supervision.

References

1. Mobley, H. L. T.; Island, M. D.; Hausinger, R. P.; *Microbiol. Rev.* **1995**, *59*, 451. [Crossref]
2. Amtul, Z.; Kausar, N.; Follmer, C.; Rozmahel, R. F.; Atta-Ur-Rahman; Kazmi, S. A.; Shekhani, M. S.; Eriksen, J. L.; Khan, K. M.; Choudhary, M. I.; *Bioorg. Med. Chem.* **2006**, *14*, 6737. [Crossref]
3. Krajewska, B.; *J. Mol. Catal. B: Enzym.* **2009**, *59*, 9. [Crossref]
4. Modolo, L. V.; da-Silva, C. J.; Brandão, D. S.; Chaves, I. S.; *J. Adv. Res.* **2018**, *13*, 29. [Crossref]
5. Ito, Y.; Shibata, K.; Hongo, A.; Kinoshita, M.; *Eur. J. Pharmacol.* **1998**, *345*, 193. [Crossref]
6. Kuehne, M. E.; He, L.; Jokiel, P. A.; Pace, C. J.; Fleck, M. W.; Maisonneuve, I. M.; Glick, S. D.; Bidlack, J. M.; *J. Med. Chem.* **2003**, *46*, 2716. [Crossref]
7. Kot, M.; Zaborska, W.; *J. Enzyme Inhib. Med. Chem.* **2003**, *18*, 413. [Crossref]
8. Kot, M.; Zaborska, W.; *J. Enzyme Inhib. Med. Chem.* **2006**, *21*, 537. [Crossref]
9. Brito, T. O.; Souza, A. X.; Mota, Y. C. C.; Morais, V. S. S.; de Souza, L. T.; de Fátima, Â.; Macedo, F.; Modolo, L. V.; *RSC Adv.* **2015**, *55*, 44507. [Crossref]
10. Kalfa, A.; Ayazoglu, E.; Colak, A.; Yasar, A.; Bekircan, O.; *Indian J. Chem.* **2019**, *58B*, 720. [Crossref]
11. Alomari, M.; Taha, M.; Imran, S.; Jamil, W.; Selvaraj, M.; Uddin, N.; Rahim, F.; *Bioorg. Chem.* **2019**, *92*, 103235. [Crossref]
12. Salar, U.; Nizamani, A.; Arshad, F.; Khan, K. M.; Fakhri, M. I.; Perveen, S.; Ahmed, N.; Choudhary, M. I.; *Bioorg. Chem.* **2019**, *91*, 103170. [Crossref]
13. Saeed, A.; Mahesar, P. A.; Channar, P. A.; Larik, F. A.; Abbas, Q.; Hassan, M.; Raza, H.; Seo, S. Y.; *Chem. Biodiversity* **2017**, *14*, e1700035. [Crossref]
14. Khan, I.; Khan, A.; Ahsan Halim, S.; Saeed, A.; Mehsud, S.; Csuk, R.; Al-Harrasi, A.; Ibrar, A.; *Int. J. Biol. Macromol.* **2020**, *142*, 345. [Crossref]
15. Deshmukh, M. N.; Burud, R.; Baldino, C.; Chan, P. C. M.; Liu, J.; *Synth. Commun.* **2003**, *33*, 3299. [Crossref]
16. Bispo, M. L. F.; Gonçalves, R. S. B.; Lima, C. H. S.; Cardoso, L. N. F.; Lourenço, M. C. S.; de Souza, M. V. N.; *J. Heterocycl. Chem.* **2012**, *49*, 1317. [Crossref]
17. Sard, H.; Meltzer, P. C.; Razdan, R. K.; *J. Heterocycl. Chem.* **1985**, *22*, 257. [Crossref]
18. Fonseca, A.; Matos, M. J.; Vilar, S.; Kachler, S.; Klotz, K. N.; Uriarte, E.; Borges, F.; *Chem. Biol. Drug Des.* **2018**, *91*, 245. [Crossref]
19. Matos, M. J.; Vilar, S.; Vazquez-Rodriguez, S.; Kachler, S.; Klotz, K.-N.; Buccioni, M.; Delogu, G.; Santana, L.; Uriarte, E.; Borges, F.; *J. Med. Chem.* **2020**, *63*, 2577. [Crossref]
20. Payra, S.; Saha, A.; Banerjee, S.; *ChemistrySelect* **2018**, *3*, 7535. [Crossref]
21. Camargo, P. G.; Fabris, M.; Nakamae, M. Y. T.; Oliveira, B. G. F.; Lima, C. H. S.; de Fátima, Â.; Bispo, M. L. F.; Macedo Jr., F.; *Chem.-Biol. Interact.* **2022**, *365*, 110045. [Crossref]
22. *GraphPad Prism*, 8.0.2; Dotmatics, Boston, U.S.A., 2019.
23. Ferreira, D. F.; *Ciênc. Agrotec.* **2014**, *38*, 109. [Crossref]
24. Frisch, M. J.; Trucks, G. W.; Schlegel, H. B.; Scuseria, G. E.; Robb, M. A.; Cheeseman, J. R.; Scalmani, G.; Barone, V.; Petersson, G. A.; Nakatsuji, H.; Li, X.; Caricato, M.; Marenich, A.; Bloino, J.; Janesko, B. G.; Gomperts, R.; Mennucci, B.; Hratchian, H. P.; Ortiz, J. V.; Izmaylov, A. F.; Sonnenberg, J. L.; Williams-Young, D.; Ding, F.; Lipparini, F.; Egidi, F.; Goings, J.; Peng, B.; Petrone, A.; Henderson, T.; Ranasinghe, D.; Zakrzewski, V. G.; Gao, J.; Rega, N.; Zheng, G.; Liang, W.; Hada, M.; Ehara, M.; Toyota, K.; Fukuda, R.; Hasegawa, J.; Ishida, M.; Nakajima, T.; Honda, Y.; Kitao, O.; Nakai, H.; Vreven, T.; Throssell, K.; Jr., J. A. M.; Peralta, J. E.; Ogliaro, F.; Bearpark, M.; Heyd, J. J.; Brothers, E.; Kudin, K. N.; Staroverov, V. N.; Keith, T.; Kobayashi, R.; Normand, J.; Raghavachari, K.; Rendell, A.; Burant, J. C.; Iyengar, S. S.; Tomasi, J.; Cossi, M.; Millam, J. M.; Klene, M.; Adamo, C.; Cammi, R.; Ochterski, J. W.; Martin, R. L.; Morokuma, K.; Farkas, O.; Foresman, J. B.; Fox, D. J.; *Gaussian*, v. 0.9, Inc., Wallingford CT, 2016.
25. Becke, A. D.; *J. Chem. Phys.* **1993**, *98*, 5648. [Crossref]
26. Lee, C.; Yang, W.; Parr, R. G.; *Phys. Rev. B* **1988**, *37*, 785. [Crossref]
27. Krishnan, R.; Binkley, J. S.; Seeger, R.; Pople, J. A.; *J. Chem. Phys.* **1980**, *72*, 650. [Crossref]
28. McLean, A. D.; Chandler, G. S.; *J. Chem. Phys.* **1980**, *72*, 5639. [Crossref]
29. da Silva, T. U.; da Silva, E. T.; Pougy, K. C.; Lima, C. H. S.; Machado, S. P.; *J. Inorg. Biochem.* **2021**, *2017*, 111359. [Crossref]

30. Balasubramanian, A.; Ponnuraj, K.; *J. Mol. Biol.* **2010**, *400*, 274. [Crossref]
31. Cunha, E. S.; Chen, X.; Sanz-Gaitero, M.; Mills, D. J.; Luecke, H.; *Nat. Commun.* **2021**, *12*, 230. [Crossref]
32. Evans, D. A.; *Angew. Chem., Int. Ed.* **2014**, *53*, 11140. [Crossref]
33. Systèmes, D.; Biovia Discovery Studio, Dassault Systèmes, France, 2016.
34. Hanwell, M. D.; Curtis, D. E.; Lonie, D. C.; Vandermeersch, T.; Zurek, E.; Hutchison, G. R.; *J. Cheminform.* **2012**, *4*, 17. [Crossref]
35. Morris, G. M.; Huey, R.; Lindstrom, W.; Sanner, M. F.; Belew, R. K.; Goodsell, Olson, A. J. D. S.; *J. Comput. Chem.* **2009**, *30*, 2785. [Crossref]
36. Trott, O.; Olson, A. J.; *J. Comput. Chem.* **2009**, *31*, 455. [Crossref]
37. Verdonk, M. L.; Cole, J. C.; Hartshorn, M. J.; Murray, C. W.; Taylor, R. D.; *Proteins: Struct., Funct., Bioinf.* **2003**, *52*, 609. [Crossref]
38. Eldridge, M. D.; Murray, C. W.; Auton, T. R.; Paolini, G. V; Mee, R. P.; *J. Comput.-Aided Mol. Des.* **1997**, *11*, 425. [Crossref]
39. Korb, O.; Stützle, T.; Exner, T. E.; *Swarm Intell.* **2007**, *1*, 115. [Crossref]
40. Mooij, W. T. M.; Verdonk, M. L.; *Proteins: Struct., Funct., Bioinf.* **2005**, *61*, 272. [Crossref]
41. DeLano, W. L.; *CCP4 Newsl. Protein Crystallogr.* **2002**, *40*, 82. [Link] accessed in August 2023
42. Vanommeslaeghe, K.; Hatcher, E.; Acharya, C.; Kundu, S.; Zhong, S.; Shim, J.; Darian, E.; Guvench, O.; Lopes, P.; Vorobyov, I.; Mackerell, A. D.; *J. Comput. Chem.* **2009**, *31*, 671. [Crossref]
43. Abraham, M. J.; Murtola, T.; Schulz, R.; Páll, S.; Smith, J. C.; Hess, B.; Lindahl, E.; *SoftwareX* **2015**, *1-2*, 19. [Crossref]
44. Huang, J.; MacKerell Jr., A. D.; *J. Comput. Chem.* **2013**, *34*, 2135. [Crossref]
45. CGenFF, https://cgenff.umaryland.edu/, accessed in August 2023.
46. Gordon, J. C.; Myers, J. B.; Folta, T.; Shoja, V.; Heath, L. S.; Onufriev, A.; *Nucleic Acids Res.* **2005**, *33*, W368. [Crossref]
47. H++, http://newbiophysics.cs.vt.edu/H++/, accessed in August 2023.
48. Mark, P.; Nilsson, L.; *J. Phys. Chem. A* **2001**, *105*, 9954. [Crossref]
49. de Santiago-Silva, K. M.; Camargo, P.; Gomes, G. F. S.; Sotero, A. P.; Orsato, A.; Perez, C. C.; Nakazato, G.; da Silva Lima, C. H.; Bispo, M.; *J. Biomol. Struct. Dyn.* **2022**, 1. [Crossref]
50. da Silva, T. U.; Pougy, K. C.; Albuquerque, M. G.; da Silva Lima, C. H.; Machado, S. P.; *J. Biomol. Struct. Dyn.* **2022**, *40*, 3481. [Crossref]
51. Bussi, G.; Donadio, D.; Parrinello, M.; *J. Chem. Phys.* **2007**, *126*, 014101. [Crossref]
52. Parrinello, M.; Rahman, A.; *J. Appl. Phys.* **1981**, *52*, 7182. [Crossref]
53. Hess, B.; Bekker, H.; Berendsen, H. J. C.; Fraaije, J. G. E. M.; *J. Comput. Chem.* **1997**, *18*, 1463. [Crossref]
54. Darden, T.; York, D.; Pedersen, L.; *J. Chem. Phys.* **1993**, *98*, 10089. [Crossref]
55. Gomes, D. E. B.; da Silva, A. W.; Lins, R. D.; Pascutti, P. G.; A., S.; *HbMap2Grace software*, Universidade Federal do Rio de Janeiro, Rio de Janeiro, Brazil, 2009.
56. Humphrey, W.; Dalke, A.; Schulten, K.; *J. Mol. Graph.* **1996**, *14*, 33. [Crossref]
57. *XMGRACE*, 5.1.19; Center for Coastal and Land-Margin Research, Oregon Graduate Institute of Science and Technology, U.S.A., 2005.
58. Kumari, R.; Kumar, R.; Lynn, A.; *J. Chem. Inf. Model.* **2014**, *54*, 1951. [Crossref]
59. Weatherburn, M. W.; *Anal. Chem.* **1967**, *39*, 971. [Crossref]
60. Ngo Nyobe, J. C.; Andiga, L. G. E.; Mama, D. B.; Amana, B. A.; Mfomo, J. Z.; Alfred, T. F. A.; Ndom, J. C.; *J. Chem.* **2019**, *2019*, ID 7684941. [Crossref]
61. Miar, M.; Shiroudi, A.; Pourshamsian, K.; Oliaey, A. R.; Hatamjafari, F.; *J. Chem. Res.* **2020**, 174751982093209. [Crossref]
62. Kappaun, K.; Piovesan, A. R.; Carlini, C. R.; Ligabue-Braun, R.; *J. Adv. Res.* **2018**, *13*, 3. [Crossref]
63. Tuccinardi, T.; Poli, G.; Romboli, V.; Giordano, A.; Martinelli, A.; *J. Chem. Inf. Model.* **2014**, *54*, 2980. [Crossref]
64. Gimeno, A.; Mestres-Truyol, J.; Ojeda-Montes, M. J.; Macip, G.; Saldivar-Espinoza, B.; Cereto-Massagué, A.; Pujadas, G.; Garcia-Vallvé, S.; *Int. J. Mol. Sci.* **2020**, *21*, 3793. [Crossref]
65. Palacio-Rodríguez, K.; Lans, I.; Cavasotto, C. N.; Cossio, P.; *Sci. Rep.* **2019**, *9*, 5142. [Crossref]
66. Albuquerque, S. O.; Barros, T. G.; Dias, L. R. S.; Lima, C. H. S.; Azevedo, P. H. R. A.; Flores-Junior, L. A. P.; dos Santos, E. G.; Loponte, H. F.; Pinheiro, S.; Dias, W. B.; Muri, E. M. F.; Todeschini, A. R.; *Eur. J. Pharm. Sci.* **2020**, *154*, 105510. [Crossref]
67. da Silva, T. U.; Pougy, K. C.; Albuquerque, M. G.; Lima, C. H. S.; Machado, S. P.; *J. Biomol. Struct. Dyn.* **2023**, *41*, 2466. [Crossref]
68. Roberts, B. P.; Miller, B. R.; Roitberg, A. E.; Merz, K. M.; *J. Am. Chem. Soc.* **2012**, *134*, 9934. [Crossref]
69. Zhou, J.-T.; Li, C.-L.; Tan, L.-H.; Xu, Y.-F.; Liu, Y.-H.; Mo, Z.-Z.; Dou, Y.-X.; Su, R.; Su, Z.-R.; Huang, P.; Xie, J.-H.; *PLoS One* **2017**, *12*, e0168944. [Crossref]
70. Fabris, M.; Nascimento-Júnior, N. M.; Bispo, M. L. F.; Camargo, P. G.; **2023**, *29*, 777. [Crossref]
71. Arora, R.; Issar, U.; Kakkar, R.; *J. Mol. Graph. Modell.* **2018**, *83*, 64. [Crossref]

Submitted: June 30, 2023
Published online: September 5, 2023